Electronic Supplementary Information (ESI) for ChemComm.
This journal is © The Royal Society of Chemistry 2021

Electronic Supplementary Information

Phosphate anion-induced silver-chalcogenide cluster-based metal organic frameworks as dual-functional catalysts for detoxifying chemical warfare agent simulant

Chun-Hua Gong,[a] Zhi-Bing Sun,[a] Man Cao,[a] Xi-Ming Luo,[a] Jie Wu,[a] Qian-You Wang,[a*] Shuang-Quan Zang,[a*] and Thomas C. W. Mak[a, b]

a Henan Key Laboratory of Crystalline Molecular Functional Materials, Henan International Joint Laboratory of Tumor Theranostical Cluster Materials, Green Catalysis Center, and College of Chemistry, Zhengzhou University, Zhengzhou 450001, China,

b Department of Chemistry, The Chinese University of Hong Kong, Hong Kong SAR 999077, China

* E-mail: zangsqzg@zzu.edu.cn; qianyouwang@zzu.edu.cn

S1. Experimental Procedures

Reagents. Chemical reagents were purchased commercially and were used without further purification. CF_3COOAg precursor was prepared by the reaction of Ag_2O and CF_3COOH in the water solvent. $[^{i}PrSAg]_n$ precursor was synthesized by the reaction of $AgNO_3$ and $^{i}PrSH$ in the presence of triethylamine in the CH_3CN and C_2H_5OH mixture solvent. H_2TCPP and ZnTCPP ligands were synthesized according to the literatures.[S1] All solvents were analytical grade reagent.

Synthesis of **ZZU-601**. A mixture of CF_3COOAg (0.1 mmol, 22 mg), $[^{i}PrSAg]_n$ (0.05 mmol, 9.2 mg) and H_2TCPP (2.53 μmol, 2 mg) was dissolved in 4 mL CH_3CN/C_2H_5OH (V:V = 1:1) to obtain a purple-red solution at room temperature. Then 30 μL 0.4 mol/L H_3PO_4 was added into the above solution. The resultant solution was sealed into 25 mL Teflon-lined autoclaves and heated at 70 ^{o}C for 24 hours. After cooling to room temperature, purple-red block crystals were obtained with a yield of 40% (based on $[^{i}PrSAg]_n$). Elemental analysis for **ZZU-601** (calculated): C, 22.42%; H, 2.64%; N, 1.26%; S, 9.21%; (found): C, 22.75%; H, 2.74%, N, 0.92%; S, 8.76%.

Synthesis of **ZZU-602**. A mixture of CF_3COOAg (0.1 mmol, 22 mg), $[^{i}PrSAg]_n$ (0.05 mmol, 9.2 mg) and ZnTCPP (2.34 μmol, 2 mg) was dissolved in 4 mL CH_3CN/C_2H_5OH (V:V = 1:1) to obtain a purple-red solution at room temperature. Then 30 μL 0.4 mol/L H_3PO_4 and 3 μL triethylamine was added into the above solution. The resultant solution was sealed into 25 mL Teflon-lined autoclaves and heated at 70 ^{o}C for 24 hours. After cooling to room temperature, purple-red block crystals were obtained with a yield of 35% (based on $[^{i}PrSAg]_n$). Elemental analysis for **ZZU-602** (calculated): C, 22.83%; H, 2.55%; N, 2.05%; S, 6.25%; (found): C, 21.55%; H, 2.78%; N, 2.22%; S, 5.84%.

Crystallographic data collection and refinement of the structure. Single-crystal X-ray diffraction measurement of **ZZU-601** and **ZZU-602** was performed on a Rigaku XtaLAB Pro diffractometer at 100 K and 200 K with Cu-Kα radiation (λ = 1.54184 Å), respectively. Data collection and reduction were performed using the program CrysAlisPro.[S2] All the structures were solved with direct methods (*SHELXS*)[S3] and refined by full-matrix least squares on F^2 using *OLEX*^{2},[S4] which utilizes the *SHELXL-2015* module.[S5] All the atoms were refined anisotropically. Hydrogen atoms were placed in calculated positions refined using idealized geometries and assigned fixed isotropic displacement parameters. ISOR, DELU, SIMU, DFIX, DANG and FLAT restraints were used for the disordered atoms. For **ZZU-601** and **ZZU-602**, the solvent mask has been used due to severely disorder of the structures or free solvent molecules in the frameworks. The crystal structures are visualized by *DIAMOND 4*. The detailed information of the crystal data, data collection and refinement results for **ZZU-601** and **ZZU-602** are summarized in Table S5. The selected H-bond data are listed in Table S6.

Characterization. Infrared spectra were obtained using recorded on a Bruker ALPHA II spectrometer with attenuated total reflection attachment in the range of 4000−400 cm^{-1}. Elemental analyses (EA) were carried out with a Perkin-Elmer 240 elemental

analyzer. Thermogravimetric (TG) analyses were performed on a SDT 2960 thermal analyzer from room temperature to 1000 ^{o}C at a heating rate of 10 ^{o}C/min under nitrogen atmosphere and oxygen atmosphere. PXRD patterns of the compounds were collected at room temperature in air on an X'Pert PRO diffractometer (Cu-Kα). A Hitachi UH4150 spectrometer was used to collect diffuse reflection spectra (DRS). Finely powdered MOF was used as a sample and $BaSO_4$ as a reference to obtain DRS spectra. The adsorption isotherms of N_2 was measured by a volumetric method using a 3H-2000Ps1 Specific surface & pore size analysis instrument at 77 K. Pore width distribution was obtained from Horvath-Kawazoe (HK) method analysis. The adsorption isotherm of CEES at 298 K were measured by gravimetric method using a Beishide 3H-2000PW Adsorption Analyzer. ^{1}H NMR and ^{31}P NMR data was recorded on a Bruker DRX spectrometer operating at 600 MHz. Electron paramagnetic resonance (EPR) spectroscopy was performed using a Bruker EMXnano system. The photoluminescence (PL) emission spectra were measured by using a Horiba FluoroLog-3 spectrofluorometer. After as-obtained MOFs was vacuum degassed at room temperature, the adsorption amounts of CEES evaporated into it were monitored by recording the sample mass while altering the pressure. Inductively Coupled Plasma-Optical Emission Spectrometer (ICP-OES) was used to evaluate the amounts of silver released from the SCC-MOFs in the supernatant of the catalytic reaction.

Photooxidation procedure of CEES. Photosensitizer (0.48 μmol porphyrin unit, 2.67 mg for **ZZU-601** and 2 mg for **ZZU-602**) was dispersed in 0.5 mL of CD_3OD in a sealed glass reactor, and then 5.6 μL (48 μmol) of CEES with 0.5 mL CD_3OD was added. After purging with O_2 or air for 15 min, the glass reactor was exposed to white LED light (Power intensity: 80 mW cm^{-2}) and the reaction process was monitored by ^{1}H NMR measurement.

Hydrolysis procedure of DECP. MOF catalysts (3 μmol porphyrin unit, 16.7 mg for **ZZU-601** or 12 mg for **ZZU-602**) was dispersed in 2 mL of CH_3OH in a sealed glass reactor, and then 9 μL (60 μmol) of DECP and 100 μL H_2O was added. The reaction process was monitored by ^{31}P NMR measurement.

Confirmation experiments for singlet oxygen production. 2,2,6,6-Tetramethyl-4-piperidone (TEMP) and 9,10-Dimethylanthracene (DMA) were selected as probes to confirm the generation of singlet oxygen, respectively. Typically, 2 mg of TEMP was dissolved in 4 mL of CH_3OH with 2.67 mg for **ZZU-601** and 2 mg for **ZZU-602** under white LED light irradiation, and the experimental results were detected via electron paramagnetic resonance (EPR) spectroscopy. 2 mg of DMA was dissolved in 4 mL of C_2H_5OH with 2.67 mg for **ZZU-601** and 2 mg for **ZZU-602** under white LED light irradiation, and the experimental results were monitored by the fluorescence emission peaks decay at 430 and 451 nm (λ_{ex} = 300 nm).

DFT simulation. All the calculations were performed within the framework of the density functional theory (DFT) as implemented in the Vienna Ab initio Software Package (VASP 5.4.4) code within the Perdew-Burke-Ernzerhof (PBE) generalized gradient approximation and the projected augmented wave (PAW) method.[S6] The cutoff energy for the plane-wave basis set was set to 400 eV. The Brillouin zone of the surface unit cell was sampled by Monkhorst-Pack (MP) grids for structure optimizations. The convergence criterion for the electronic self-consistent iteration and force was set to 10^{-5} eV and 0.01 eV/Å, respectively.

Data availability. Data supporting the findings of this manuscript are available from the corresponding authors upon reasonable request. The X-ray crystallographic coordinates for structures reported in this article have been deposited at the Cambridge Crystallographic Data Centre (CCDC) under deposition number CCDC: 2153380 (**ZZU-601**) and 2153381 (**ZZU-602**).

S2. Supplementary Figures and Tables

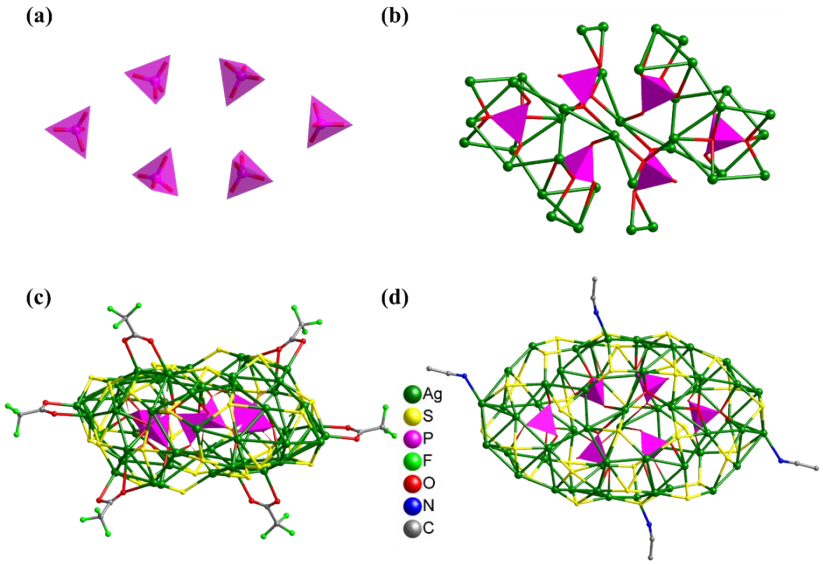

Figure S1. Structure of Ag_{54} cluster node in **ZZU-601**. (a) Arrangement of internal six [PO_4] anion template units. (b) The coordination between [PO_4] units and Ag atoms of the 54-Ag shell. (c) Coordination modes of six CF_3COO^- ligands and Ag_{54} cluster. (d) Coordination mode of CH_3CN molecules and Ag_{54} cluster.

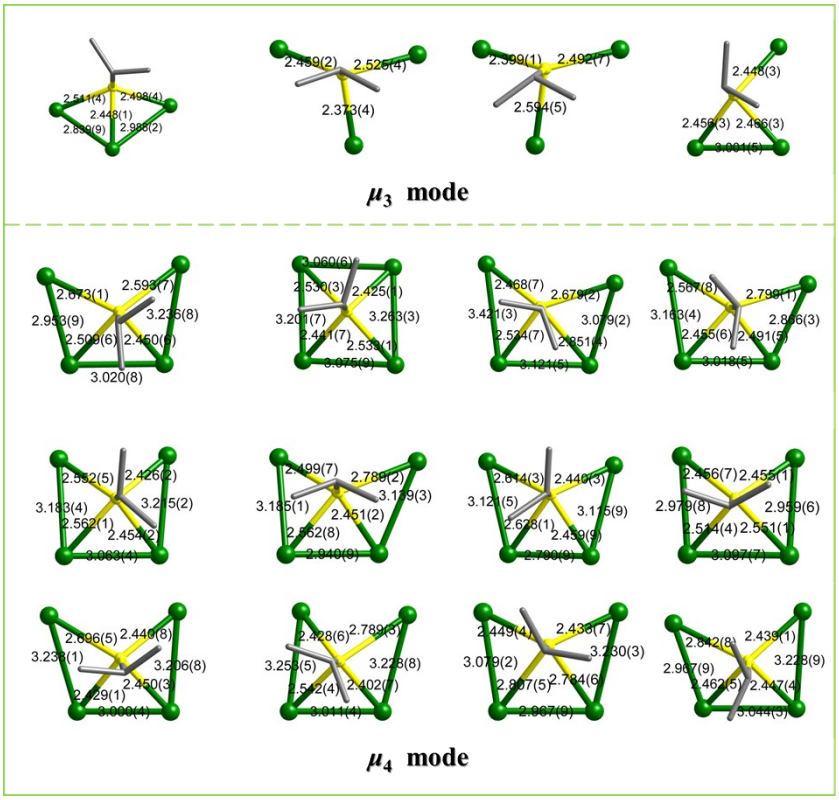

Figure S2. Coordination modes of S atoms from $^{i}PrS^{-}$ ligands in **ZZU-601**.

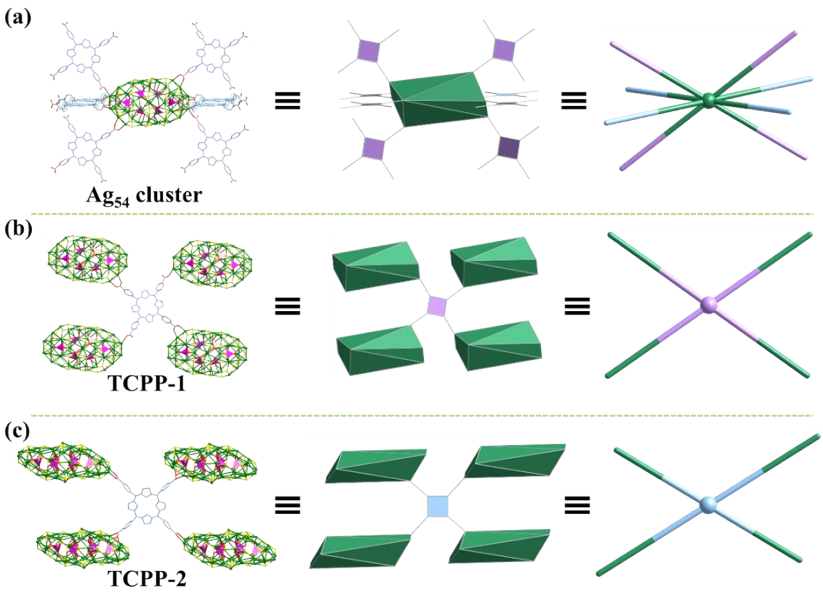

Figure S3. (a) Coordination environment of Ag_{54} cluster as eight-connected node in **ZZU-601**. (b and c) Coordination environment of H_2TCPP ligands (TCPP-1 and TCPP-2) as four-connected linkers in **ZZU-601**.

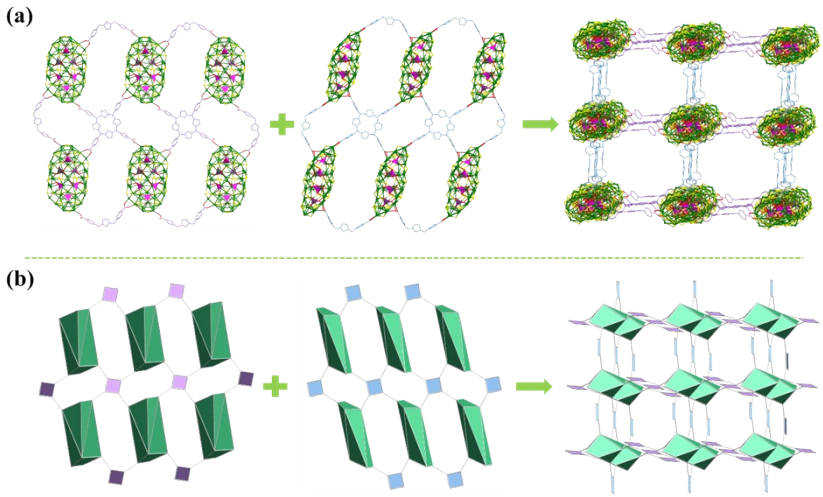

Figure S4. 2D nets of Ag54 cluster bridged by TCPP-1 and TCPP-2 ligands to form 3D frameworks in ball-and-stick mode (a) and polyhedron mode (b) in **ZZU-601**, respectively.

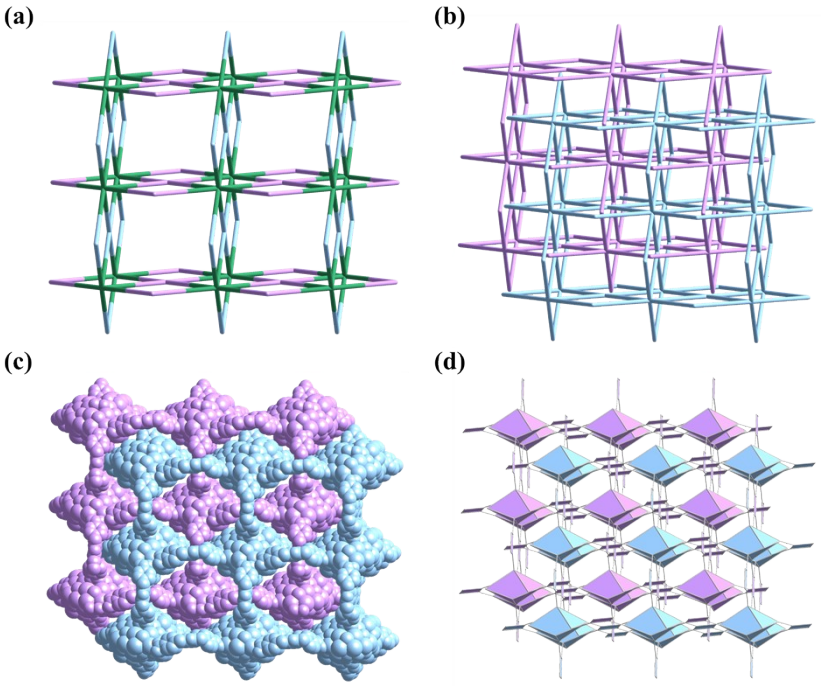

Figure S5. (a and b) The 3D *scu* topology net and the double interpenetrating 3D net in **ZZU-601**. (c and d) The double interpenetrating 3D structures in space-filling mode and polyhedron mode in **ZZU-601**, respectively.

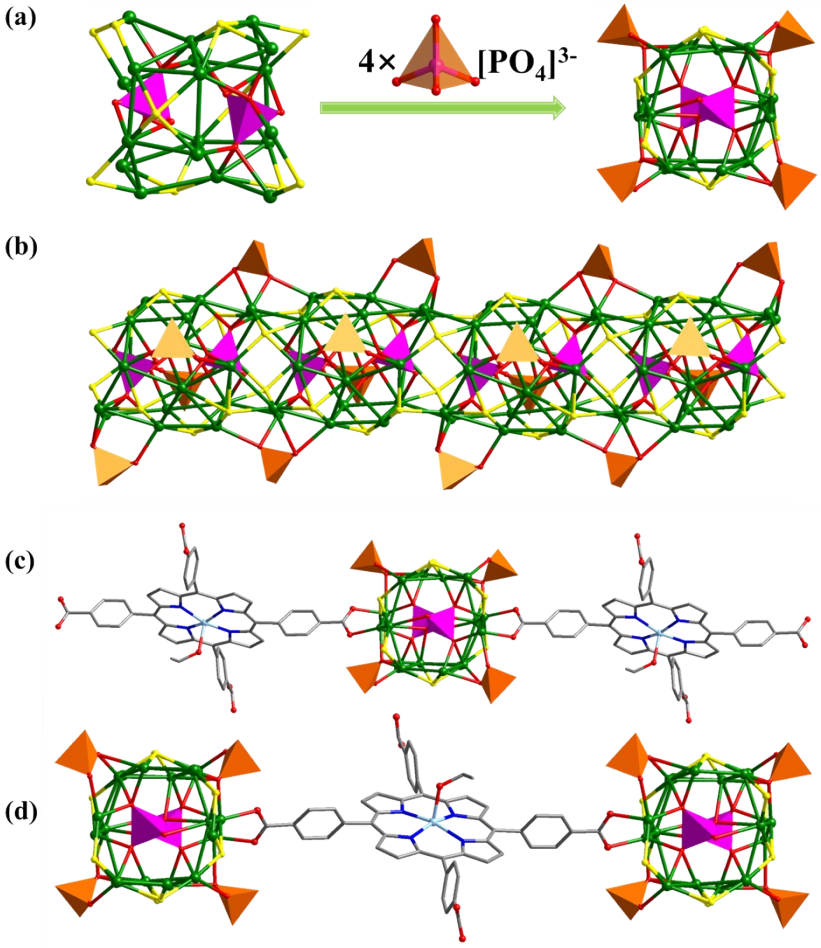

Figure S6. (a) The structure of 2[HPO_4]@Ag_{18}(^{i}PrS)$_{10}$(H_2PO_4)$_4$ unit in **ZZU-602**. (b) The infinite 1D Ag-S rod. (c) The coordination environment of Ag_{18} unit. (d) The coordination environment [H_2ZnTCPP(C_2H_5OH)] ligand.

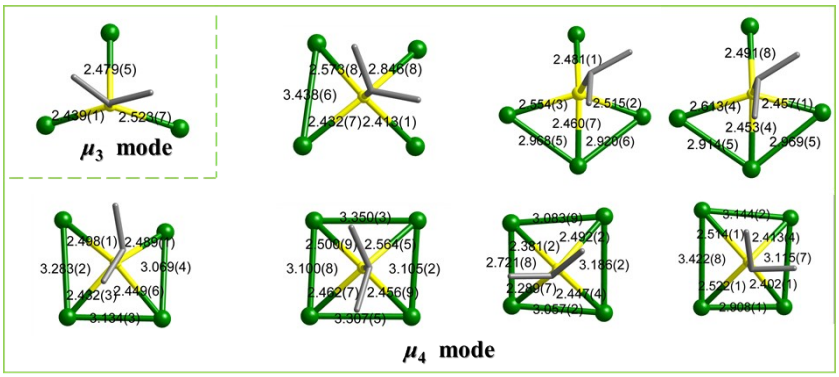

Figure S7. Coordination modes of S atoms from ^{i}PrS$^-$ ligands in **ZZU-602**.

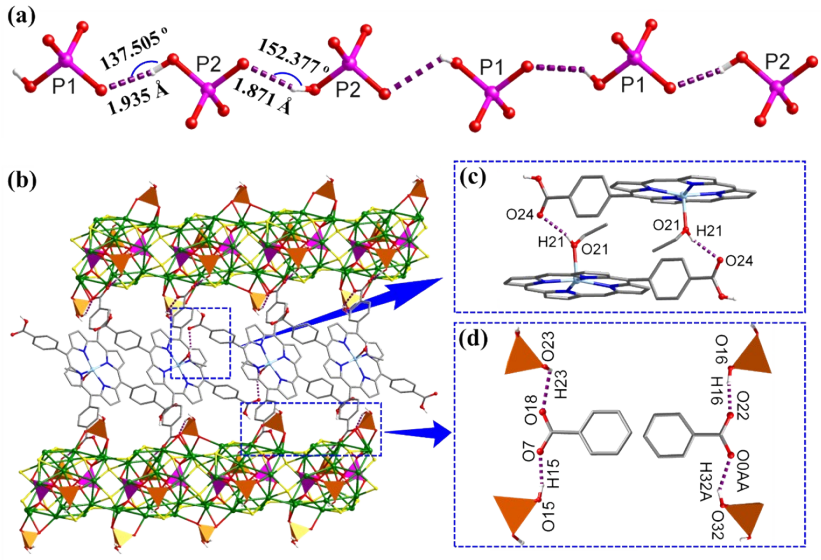

Figure S8. The intramolecular hydrogen bonds in **ZZU-602**. (a) The H-bond interaction among $[H_xPO_4]^{(3-x)-}$ anions in the Ag-S rod. (b) The H-bond interaction in the 2D framework. (c) Partial magnification of the H-bond interaction from the adjacent ZnTCPP linkers. (d) Partial magnification of the H-bond interaction between $[H_xPO_4]^{(3-x)-}$ anions and ZnTCPP linkers.

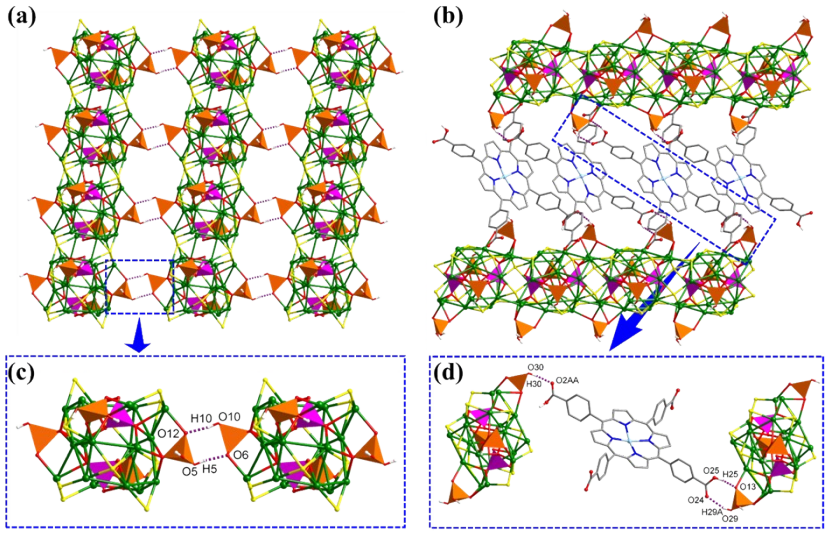

Figure S9. The intermolecular hydrogen bonds in **ZZU-602**. (a) Intermolecular hydrogen bonds of the adjacent Ag-S rods to form 2D net. (b) Intermolecular hydrogen bonds between the outer $[H_xPO_4]^{(3-x)-}$ anion of the Ag-S rods and ZnTCPP linkers to form 2D net. (c) Partial magnification of the H-bond interaction among the adjacent Ag-S rods. (d) Partial magnification of the H-bond interaction between the outer $[H_xPO_4]^{(3-x)-}$ anion of the Ag-S rods and ZnTCPP linkers.

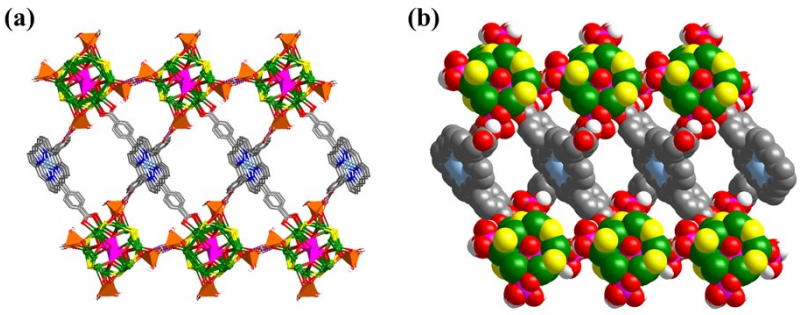

Figure S10. (a) 3D supramolecular network of **ZZU-602** in ball-stick mode through intermolecular hydrogen bonds. (b) 3D supramolecular network **ZZU-602** in space-filling mode through intermolecular hydrogen bonds.

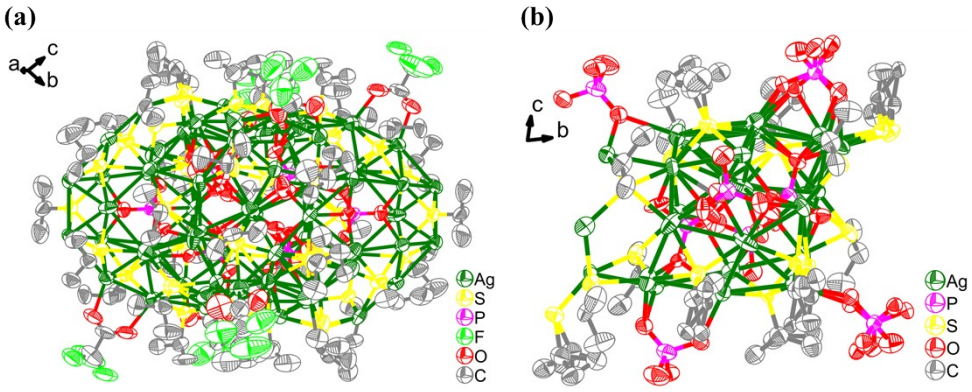

Figure S11. (a) The ellipsoid diagram of Ag_{54} cluster unit in **ZZU-601**. (b) The ellipsoid diagram of Ag_{18} cluster unit in **ZZU-602**.

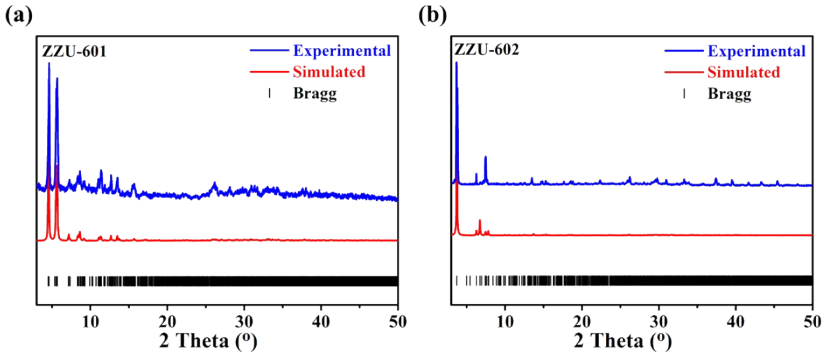

Figure S12. PXRD patterns of **ZZU-601** (a) and **ZZU-602** (b).

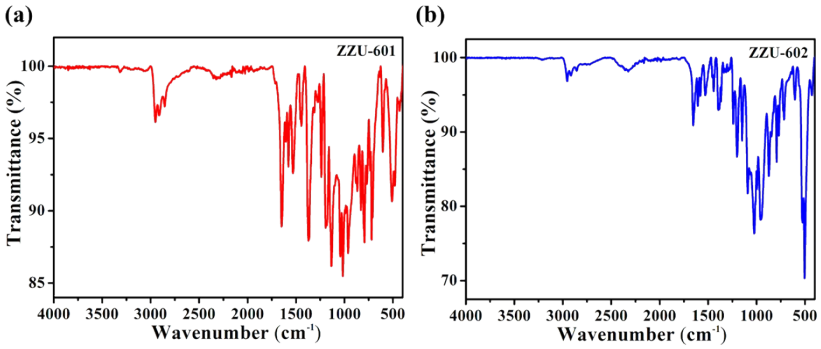

Figure S13. The IR spectra of **ZZU-601** (a) and **ZZU-602** (b).

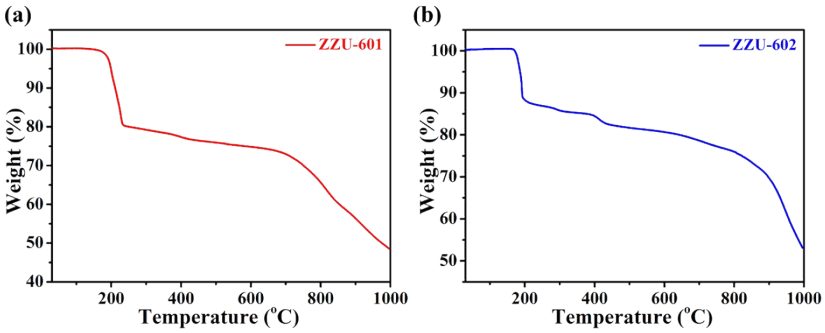

Figure S14. The thermogravimetric curves of **ZZU-601** (a) and **ZZU-602** (b) under N_2 atmosphere.

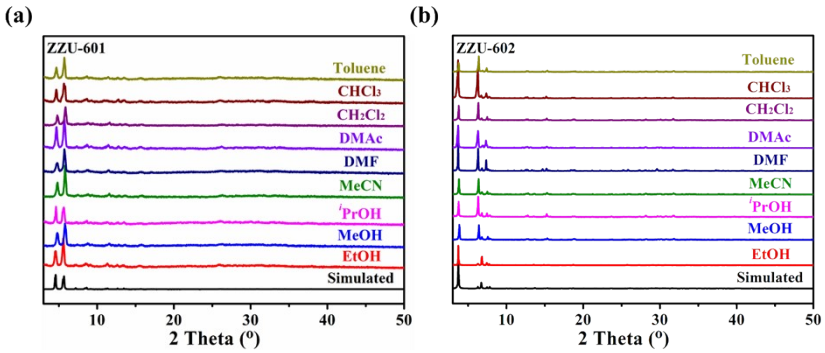

Figure S15. The chemical stability of **ZZU-601** (a) and **ZZU-602** (b).

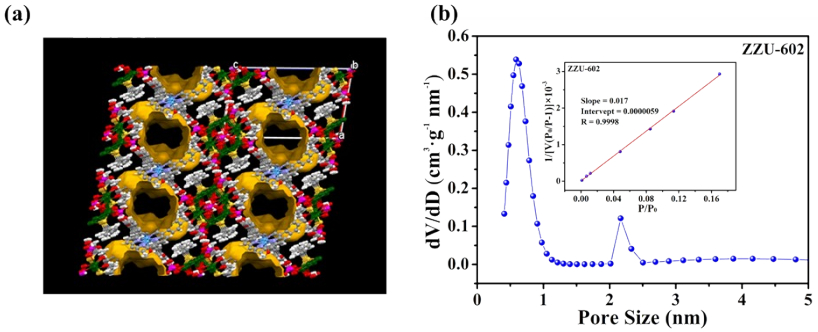

Figure S16. (a) Schematic diagram of channels in **ZZU-602**. (b) Pore size distribution profile based on nonlocal density function theory (NLDFT) of **ZZU-602**. Inset: Selected BET Plots of **ZZU-602** for BET surface area calculation based on N_2 adsorption isotherm at 77 K.

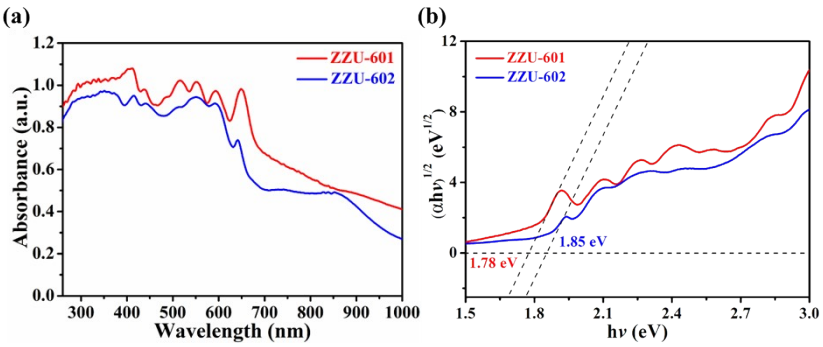

Figure S17. (a) UV-Vis diffuse reflectance spectra of **ZZU-601** and **ZZU-602** at room-temperature. (b) Tauc plot displaying the band gap of **ZZU-601** and **ZZU-602**.

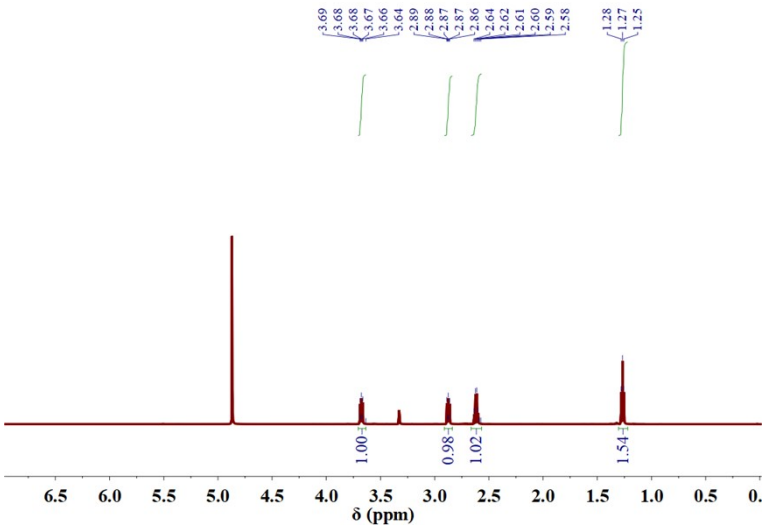

Figure S18. ^{1}H NMR spectrum of CEES reaction substrate in CD_3OD.

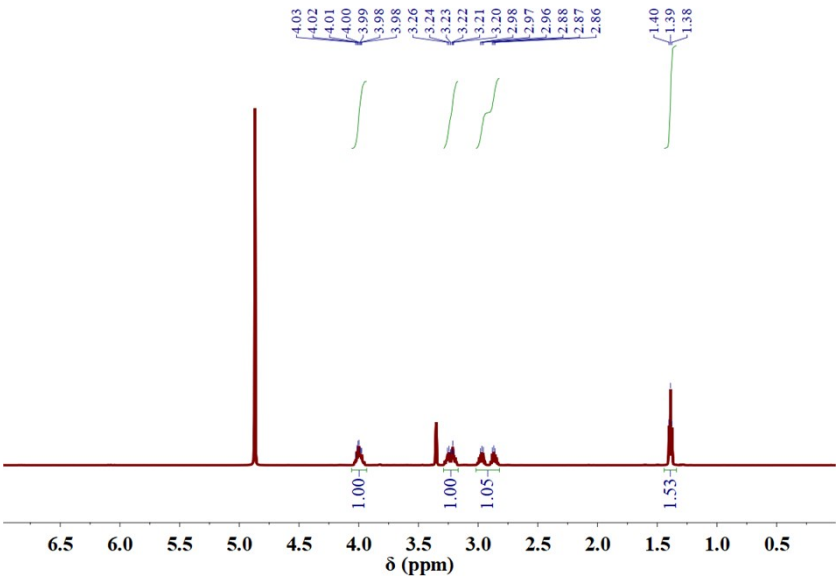

Figure S19. ^{1}H NMR spectrum of CEESO oxidation product in CD_3OD.

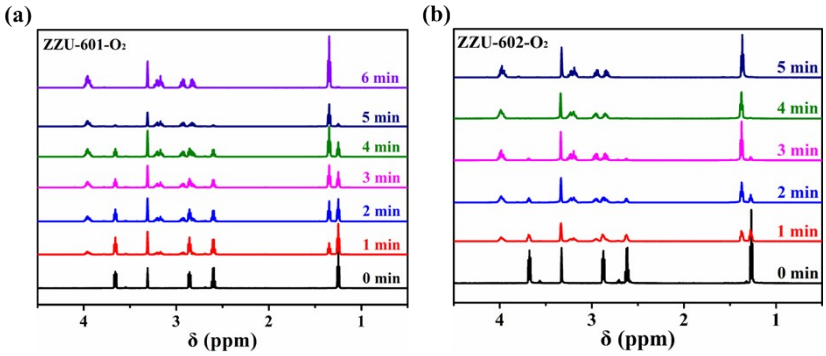

Figure S20. (a) ^{1}H NMR spectra monitoring of the photooxidation reaction of CEES by **ZZU-601** under O_2 atmosphere and white LED irradiation. (b) ^{1}H NMR spectra monitoring of the photooxidation reaction of CEES by **ZZU-602** under O_2 atmosphere and white LED irradiation.

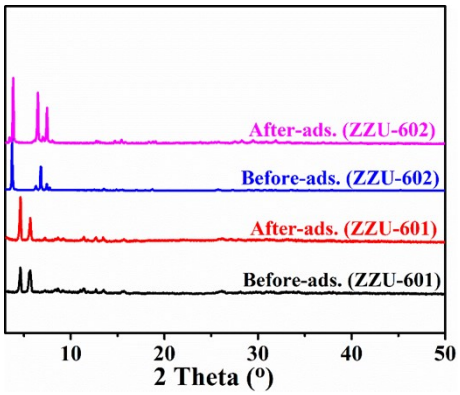

Figure S21. PXRD patterns before and after CEES adsorption of **ZZU-601** and **ZZU-602**.

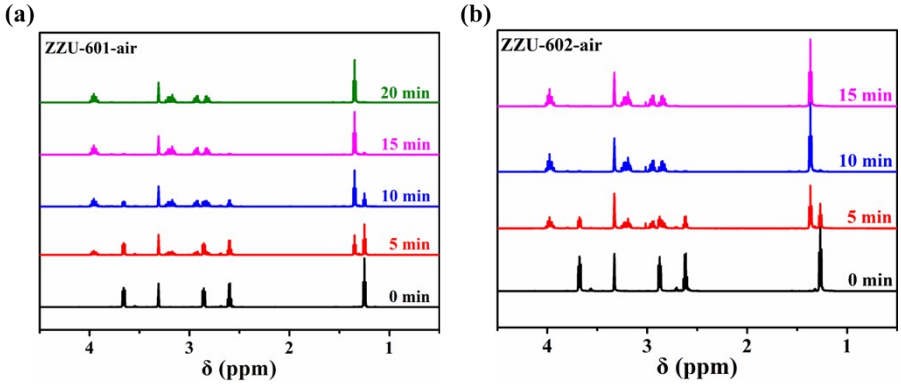

Figure S22. (a) ^{1}H NMR spectra monitoring of the photooxidation reaction of CEES by **ZZU-601** under air atmosphere and white LED irradiation. (b) ^{1}H NMR spectra monitoring of the photooxidation reaction of CEES by **ZZU-602** under air atmosphere and white LED irradiation.

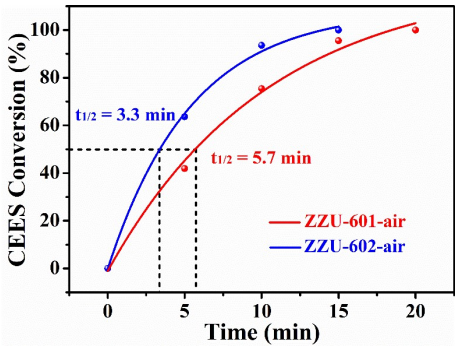

Figure S23. Conversion of the CEES photooxidation in the presence of **ZZU-601** and **ZZU-602** under air atmosphere.

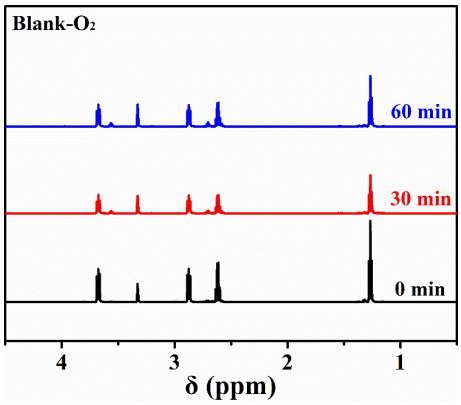

Figure S24. ^{1}H NMR spectra monitoring of the photooxidation reaction of CEES under O_2 atmosphere and white LED irradiation without any catalyst.

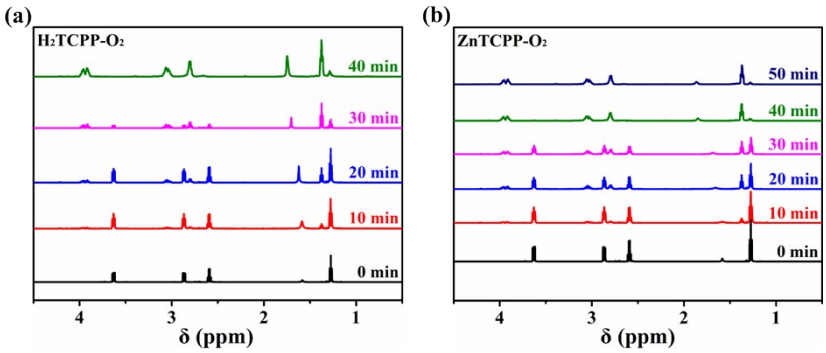

Figure S25. (a) ^{1}H NMR spectra monitoring of the photooxidation reaction of CEES by H_2TCPP ligand under O_2 atmosphere and white LED irradiation. (b) ^{1}H NMR spectra monitoring of the photooxidation reaction of CEES by ZnTCPP ligand under O_2 atmosphere and white LED irradiation.

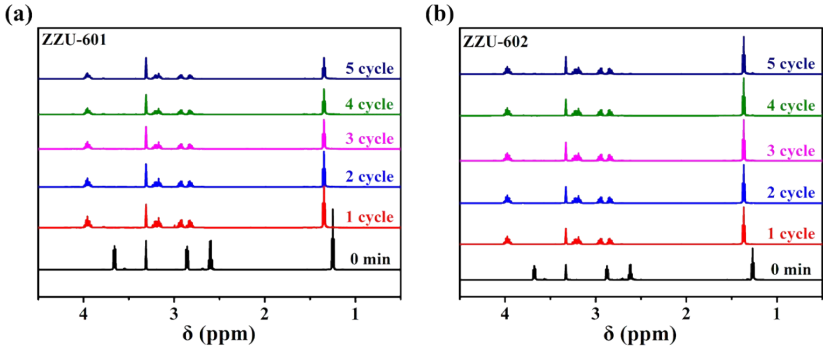

Figure S26. (a) ^{1}H NMR spectra monitoring of the photooxidation cycling reaction of CEES by **ZZU-601**. (b) ^{1}H NMR spectra monitoring of the photooxidation cycling reaction of CEES by **ZZU-602**.

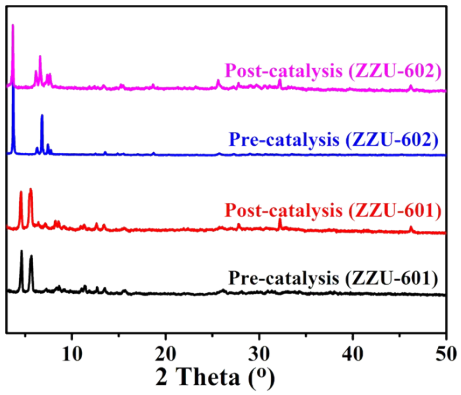

Figure S27. PXRD patterns before and after CEES photooxidation of **ZZU-601** and **ZZU-602**.

Table S1. Comparison of the required time under different experimental conditions in CEES complete photooxidation in this work.

Entry	Photosensitizer	O_2/Air	Light	The time with 100% conversion rate
1	**ZZU-601**	O_2	ON	6 min
2	**ZZU-601**	Air	ON	20 min
3	**ZZU-602**	O_2	ON	5 min
4	**ZZU-602**	Air	ON	15 min
5	H_2TCPP	O_2	ON	40 min
6	ZnTCPP	O_2	ON	50 min
7	---[a]	O_2	ON	---[b]

[a] Control experiment without photosensitizer. [b] CEES was not oxidized within 60 minutes.

Table S2. Comparison of the photo-oxidative efficiency of reported MOFs with porphyrin unit in CEES photooxidation under O_2 atmosphere.

Photosensitizer	Photosensitizer Loading	Half-life (min)	Light source (mW cm^{-2})	Reference

PCN-222	0.5 %	13 26 33	Blue (325) White (310) Red (160)	S7a
PCN-222/MOF-545	0.5%	11	Blue	S7b
Ag_{12}TPyP	1%	1.5	White (80)	S8
Fe-TCPP-La Ni-TCPP-La Zn-TCPP-La Mn-TCPP-La Co-TCPP-La	1%	2.5 3.5 4 5 5.5	Blue	S7c
Al-PMOF	0.7%	16	Blue	S7d
ZZU-601	1%	2.3	White (80)	This work
ZZU-602	1%	1.1	White (80)	This work

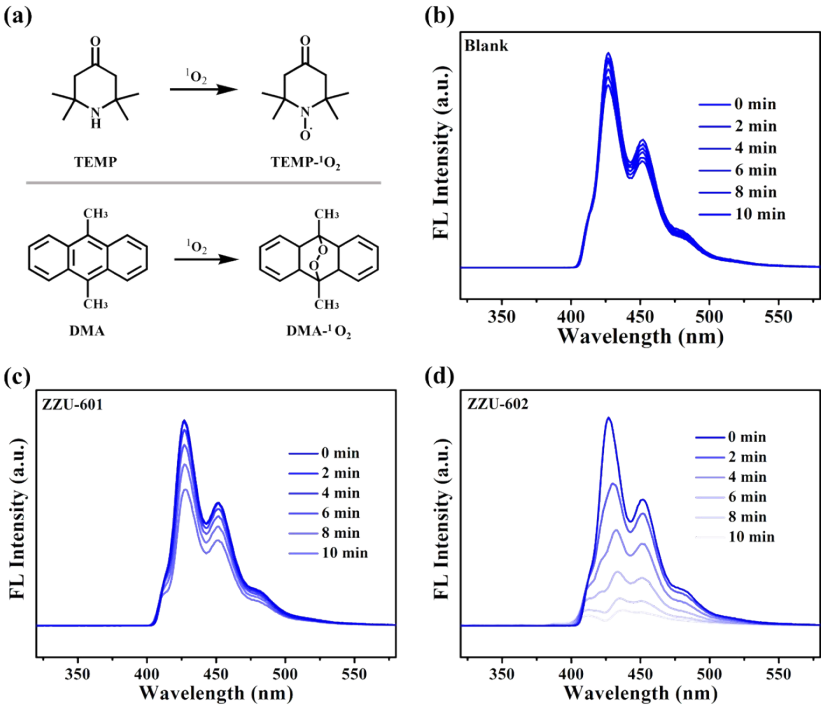

Figure S28. (a) Photooxidation process of TEMP and DMA as probes in the presence of singlet oxygen ($^1O_2$). (b) Fluorescence spectra of DMA without any catalyst upon light irradiation. (c) Fluorescence spectra of DMA in the presence of **ZZU-601** upon light irradiation. (d) Fluorescence spectra of DMA in the presence of **ZZU-602** upon light irradiation.

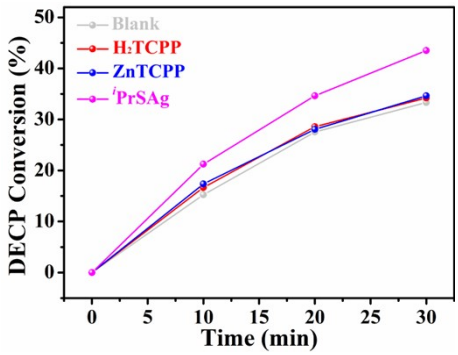

Figure S29. Conversion of DECP hydrolysis in the presence of ^{i}PrSAg, H_2TCPP, ZnTCPP and no catalyst, respectively.

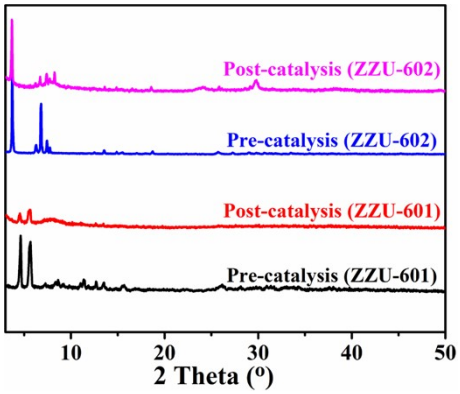

Figure S30. PXRD patterns before and after DECP hydrolysis of **ZZU-601** and **ZZU-602** in 30 min.

Table S3. Comparison of DECP hydrolysis by the reported MOFs under the same reaction conditions.

Catalyst	Time (min)	Conversion (%)
ZZU-601	30 min	48
ZZU-602	30 min	61
HKUST-1	30 min	90
Uio-66	30 min	100

Table S4. The leaching amounts of silver ions in the supernatant after the catalytic reaction using ICP-OES.

Catalyst	**ZZU-601**	**ZZU-602**	**ZZU-601**	**ZZU-602**
Catalytic substrate	CEES	CEES	DECP	DECP
The total mass of silver in the catalyst (mg)	1.39	0.95	8.73	5.68
The content of silver in the supernatant (mg/L)	3.4	4.2	3.9	6.9
The mass of silver in the supernatant (mg)	3.42×10^{-3}	4.22×10^{-3}	8.22×10^{-3}	1.46×10^{-2}
The leaching amounts of silver ions (%)	0.24	0.44	0.09	0.25

Table S5. Crystal data and structure refinements for **ZZU-601** and **ZZU-602**.

Identification code	**ZZU-601**	**ZZU-602**
CCDC number	2153380	2153381
Empirical formula	$C_{208}H_{292}Ag_{54}F_{18}N_{10}O_{52}P_6S_{32}$	$C_{78}H_{104}Ag_{18}N_6O_{33}P_6S_8Zn$
Formula weight	11143.22	4103.03
Temperature/K	100	200
Crystal system	triclinic	triclinic
Space group	$P\bar{1}$	$P\bar{1}$
a/Å	20.7199(8)	14.4671(2)
b/Å	21.3162(9)	18.4226(2)
c/Å	21.6663(15)	24.9929(3)
α/°	67.507(5)	74.157(10)
β/°	70.652(5)	78.318(10)
γ/°	71.542(4)	81.167(10)
Volume/Å^3	8141.8(8)	6241.14(14)
Z	1	2
ρ_{calc} / g·cm^{-3}	2.273	2.183
μ/mm^{-1}	28.133	24.815
F(000)	5328.0	3856.0
Radiation	CuK*α* (*λ* = 1.54184)	CuK*α* (*λ* = 1.54184)
2θ range for data collection/°	5.56 to 148.972	5.014 to 147.78

Index ranges	-25 ≤ h ≤ 23 -26 ≤ k ≤ 25 -26 ≤ l ≤ 20	-15 ≤ h ≤ 18 -22 ≤ k ≤ 22 -30 ≤ l ≤ 31
Reflections collected	67854	67884
Independent reflections	31427	24364
R_{int}	0.0866	0.0565
R_{sigma}	0.1179	0.0596
Data/restraints/parameters	31427/461/1999	24364/545/1515
Goodness-of-fit on F^2	1.057	1.013
R_1[a], wR_2[b] [I>=2σ (I)]	R_1 = 0.0902, wR_2 = 0.2419	R_1 = 0.0984, wR_2 = 0.2351
R_1[a], wR_2[b] [all data]	R_1 = 0.1458, wR_2 = 0.2889	R_1 = 0.1100, wR_2 = 0.2418
Largest diff. peak/hole / e Å^{-3}	2.49/-1.98	2.35/-1.99

[a]$R_1 = \sum||F_o| - |F_c||/\sum|F_o|$. [b]$wR_2=\{\sum[w(F_o^2 - F_c^2)^2]/\sum[w(F_o^2)^2]\}^{1/2}$, $w = 1/[\sigma^2(F_o^2) +(0.1000P)^2]$ where $P = (F_o^2 + 2F_c^2)/3$.

Table S6. Hydrogen bond data used for **ZZU-602**.

Type	Donor–H···Acceptor	D–H (Å)	H···A (Å)	D···A (Å)	D–H···A (°)
Intra	O14–H14···O14	0.82	1.871	2.626	152.377
Intra	O15–H15···O7	0.82	1.849	2.637	160.697
Intra	O16–H16···O22	0.82	1.780	2.593	151.378
Intra	O19–H19···O11	0.82	1.935	2.600	137.505
Intra	O21–H21···O24	0.85	2.045	2.831	153.677
Intra	O32–H32A···O0AA	0.82	2.085	2.819	148.990
Inter	O5–H5···O6	0.82	1.746	2.554	167.762
Inter	O10–H10···O12	0.82	1.756	2.556	164.645
Inter	O25–H25···O13	0.82	1.668	2.474	165.813
Inter	O29–H29A···O24	0.83	2.128	2.923	161.620
Inter	O30–H30···O2AA	0.82	1.882	2.682	165.105

S3. References

S1 a) H.-Q. Xu, J. Hu, D. Wang, Z. Li, Q. Zhang, Y. Luo, S.-H. Yu and H.-L. Jiang, *J. Am. Chem. Soc.*, 2015, **137**, 13440–13443; b) D. Feng, Z.-Y. Gu, J.-R. Li, H.-L. Jiang, Z. Wei and H.-C. Zhou, *Angew. Chem. Int. Ed.*, 2012, **51**, 10307–10310.

S2 a) CrysAlisPro, Version 1.171.36.31. Agilent Technologies Inc., Santa Clara, CA, USA 2012; b) O. D. Rigaku, CrysAlisPro Software System, Version 1.171.38.41k,

Rigaku Coorporation, Oxford, UK 2015.

S3 G. M. Sheldrick, *Acta Cryst. A*, 2008, **64**, 112-122.

S4 O. V. Dolomanov, L. J. Bourhis, R. J. Gildea, J. A. K. Howard and H. Puschmann, *J. Appl. Cryst.*, 2009, **42**, 339-341.

S5 G. M. Sheldrick, *Acta Cryst. C*, 2015, **71**, 3-8.

S6 a) J. P. Perdew, K. Burke and M. Ernzerhof, *Phys. Rev. Lett.*, 1996, **77**, 3865-3868; b) B. Hammer, L. B. Hansen and J. K. Nørskov, *Phys. Rev. B*, 1999, **59**, 7413-7421; c) P. E. Blöchl, *Phys. Rev. B*, 1994, **50**, 17953-17979; d) G. Kresse and D. Joubert, *Phys. Rev. B*, 1999, **59**, 1758-1775.

S7 a) Y. Liu, A. J. Howarth, J. T. Hupp and O. K. Farha, *Angew. Chem. Int. Ed.*, 2015, **54**, 9001–9005; b) C. T. Buru, M. B. Majewski, A. J. Howarth, R. H. Lavroff, C.-W. Kung, A. W. Peters, S. Goswami and O. K. Farha, *ACS Appl. Mater. Interfaces*, 2018, **10**, 23802–23806; c) Z.-H. Long, D. Luo, K. Wu, Z.-Y. Chen, M.-M. Wu, X.-P. Zhou and D. Li, *ACS Appl. Mater. Interfaces*, 2021, **13**, 37102–37110; d) D. T. Lee, J. D. Jamir, G. W. Peterson and G. N. Parsons, *Matter*, 2020, **2**, 404–415.

S8 M. Cao, R. Pang, Q.-Y. Wang, Z. Han, Z.-Y. Wang, X.-Y. Dong, S.-F. Li, S.-Q. Zang and T. C. W. Mak, *J. Am. Chem. Soc.,* 2019, **141**, 14505–14509.